High-quality multiple T_2(*) contrast MR images from low-quality multi-echo images using temporal-domain denoising methods

Ung Jang and Dosik Hwang[a)]
School of Electrical and Electronic Engineering, College of Engineering, Yonsei University, 262 Seongsanno, Seodaemun-gu, Seoul 120-749, Korea

(Received 19 July 2011; revised 11 November 2011; accepted for publication 1 December 2011; published 29 December 2011)

Purpose: The aim of this study was to develop an effective postprocessing method to increase the signal-to-noise ratio in successive multi-echo magnetic resonance (MR) images acquired at multiple time points and generate high-quality multiple T_2(*) contrast images from low-quality multi-echo images.
Methods: Successive multi-echo MR images were acquired at multiple time points using a multigradient-recalled echo sequence at 3T and rearranged so that each pixel in the images had its own decay signal in the temporal-domain. Two different denonising approaches were implemented in the temporal-domain: (1) In a filtering approach, conventional low-pass filter, median filter, and anisotropic diffusion filter were applied to the decay signals to reduce random noise; (2) In a model-based approach, a non-negative least squares algorithm was applied for fitting to MR relaxation model for decay signals. Numerical simulations and *in vivo* experiments were conducted. The denoised images were compared to each other by visual inspection and analysis of mean square error (MSE) and contrast-to-noise ratio (CNR) on several regions of interest.
Results: Our proposed method suppressed noise in each multi-echo images without introducing spatial artifacts. This was a natural consequence of the proposed denoising process, which was performed in the temporal-domain and did not use any cross-pixel operation. MSEs decreased by a factor of 5.4–7.9 and CNRs increased by a factor of 5 in simulation studies. The results were consistent with the *in vivo* findings. Random noise in the images was effectively reduced and high-quality multiple T_2(*) contrast images were obtained.
Conclusions: This study demonstrated that denoising methods in the temporal-domain can effectively suppress noise in the spatial domain, and increase signal-to-noise ratio (SNR) for each image of different T_2(*) weights at multiple time points, resulting in multiple high-quality T_2(*) contrast images. [DOI: 10.1118/1.3671934]

Key words: magnetic resonance imaging, noise reduction, temporal filtering, non-negative least squares algorithm, low-pass filter, relaxation model, multiple contrasts

I. INTRODUCTION

Magnetic resonance imaging (MRI) has become one of the most popular medical imaging modalities for disease diagnosis because it noninvasively provides high-resolution and high-contrast images. However, its spatial and temporal resolution and contrast are often degraded by a low signal-to-noise ratio (SNR). Efforts to improve the SNR by developing better systems include high-field MRI, surface coils, and multiple transmitting and receiving coils, and developing postprocessing algorithms such as linear low-pass filter (LPF),[1] median filter (MF),[2] and anisotropic diffusion filter (ADF) (Ref. 3) to reduce noise in magnetic resonance (MR) images. Acquisition methods and selection of optimal scan parameters have also been investigated as ways to obtain high-SNR images. A simple way of increasing the SNR is to increase scan time, since the SNR of MR images is proportional to acquisition time. However, when the scan time is limited, the number of images to be acquired should be reduced to increase SNR. Nonetheless, acquiring multiple T_2(*)-weighted images is common, which is helpful for diagnosis, since different T_2(*)-weighted images provide different contrasts between tissues. Multiple T_2(*)-weighted images are acquired for special purposes such as improved diagnosis, quantification of water or myelin contents,[4,5] high-quality venography,[6,7] cervical spinal cord imaging,[8] and orthopedic imaging.[9] A set of multiple T_2(*)-weighted images can form successive multi-echo MR images, which are a series of MR images acquired at different echo times. However, many of these images tend to have a low SNR because high sampling rates are used to reduce the total scan time. Therefore, an efficient denoising method for successive multi-echo MR images that produces high-quality multiple T_2(*) contrast images from low-quality images is needed.

Conventional denoising approaches are mostly based on spatial filters such as LPF, MF, and ADF. These spatial filters can effectively reduce noise, but introduce spatial artifacts.[1,3] For examples, LPF reduces noise but smoothes image details such as small structures and edges. This blurring artifact can be reduced by the application of nonlinear filters. MF is a nonlinear filter and has been widely used in many image-processing applications. It can preserve

relatively large edges while suppressing noise. However, small structures and fine details tend to be degraded by MF. ADF is very effective in preserving fine details while suppressing noise. It filters local areas adaptively depending on their structural information. However, ADF introduces an artificial appearance, such as caused by staircasing artifacts, due to its nonlinear process.[2,3] For proper diagnosis, both loss of fine structures and the introduction of an artificial appearance should be avoided. Therefore, the available spatial filters have limitations for medical imaging because they introduce undesirable artifacts.

These artifacts exist primarily because the filtering processes are performed in the spatial domain of the images. The intensity of a single-pixel influences the intensities of its neighboring pixels, which introduces spatial artifacts. As long as filtering is performed in the spatial domain, removing these artifacts is difficult.

In this paper, we propose a new denoising approach in which the conventional filters and a model-based method are performed in the temporal rather than the spatial domain, to avoid spatial artifacts. Since the denoising process does not involve the spatially adjacent pixels, the denoising result is naturally free of spatial artifacts.

In successive multi-echo MR images, the intensity at a specific voxel follows a slowly varying decay function of echo time. Therefore, conventional filtering techniques can be applied to the decay signals, or in the temporal-domain, which reduces noise. Furthermore, these decay signals can be modeled based on MR physics, specifically a $T_2(*)$ relaxation model in the temporal-domain, which can also result in noise reduction. In contrast to the spatial domain, denoising in the temporal-domain introduces very few of the aforementioned artifacts since it does not use spatial information. In other words, denoising in the temporal-domain at a specific voxel does not affect neighboring voxels in the spatial domain. The proposed temporal denoising approach produced high-quality $T_2(*)$-weighted images comparable to conventionally acquired single $T_2(*)$-weighted images, but also produced additional different $T_2(*)$ contrast images with the same imaging time.

Simulations and *in vivo* experiments were conducted using the proposed denoising method. Visual inspections of the denoised images, the analysis of the mean square error (MSE) and contrast-to-noise ratio (CNR) on several regions of interest (ROI) demonstrated the effectiveness of the proposed method.

II. METHODS

II.A. Data acquisition

For *in vivo* experiments, normal volunteers were scanned with a multigradient echo (MGRE) sequence and conventional gradient echo (GRE) sequence using a 3T Siemens MRI system (Erlangen, Germany). GRE sequence parameters were repetition time (TR) = 49 ms, echo time (TE) = 38.7 ms, flip angle = 17°, field of view (FOV) = 215 × 215 mm^2, matrix resolution = 512 × 512, slice thickness = 1.6 mm, and bandwidth = 80 Hz/Px. MGRE sequence parameters were TR = 95 ms, TE_1 = 5.67 ms, echo spacing (ES) = 5.51 ms, flip angle = 27°, FOV = 215 × 215 mm^2, matrix resolution = 512 × 512, slice thickness = 1.6 mm, bandwidth = 444 Hz/Px, and sixteen echoes were acquired. The seventh echo time was 38.73 ms. Generalized autocalibrating partially parallel acquisitions (GRAPPA) (Ref. 10) was applied to multi-echo sequences to reduce acquisition time by a factor of two. GRE sequence total acquisition time was 13 min 24 s, and MGRE sequence total acquisition time was 14 min 13 s.

in vivo data were acquired to determine if the proposed denoising methods could effectively suppress noise in single images and preserve small details without blurring effects. The study was approved by the Institutional Review Board of Yonsei University, and written informed consent was obtained.

II.B. Simulation of synthetic data

Simulations were performed with synthetic image data to assess the effectiveness of the proposed method. The synthetic data modeled a single slice multi-echo image dataset that contained uniform normal white matter (WM) as a background and nine focal lesions as shown in Fig. 1(a). Diameters for lesions 1–9 were 1, 3, 5, 7, 9, 11, and 17 pixels, respectively.

Image matrix size was 128 × 128, and the number of echoes was 100, with first echo time (TE_1) = 3 ms and ES = 1 ms. Intensities at different echo times were generated for normal *WM* [Eq. (1a)] and lesions [Eq. (1b)] according to the following decay functions:

$$S_{WM}(TE) = 1000 \times e^{-TE/10} + 5000 \times e^{-TE/80} + 4000 \times e^{-TE/100}, \quad (1a)$$

$$S_{\text{lesion}}(TE) = 5500 \times e^{-TE/80} + 4500 \times e^{-TE/100}. \quad (1b)$$

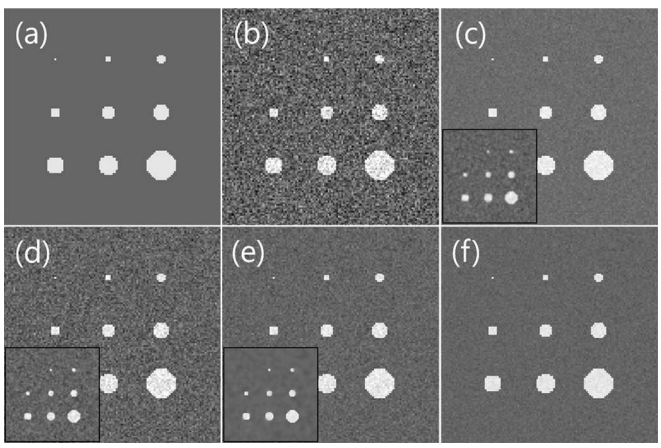

FIG. 1. Comparison of temporally denoised images at TE = 22 ms. Conventional filters and the model-based method were applied to the simulated dataset in the temporal-domain. True image (a), noisy image with SNR = 80 dB (b), and denoised images by temporal filtering with LPF (c), MF (d), ADF (e), and the model-based method (f). All methods resulted in substantial noise reduction with high contrast. Small inset images in (c)–(e) are spatially denoised images with LPF, MF, and ADF, respectively, to show spatial artifacts observed in spatial denoising scheme.

TABLE I. MSE of the temporally denoised images at three different echo times.

TE(ms)	Reference	LPF	MF	ADF	Modeling
27	0.1235	0.0270	0.0721	0.0431	0.0228
52	0.1242	0.0268	0.0611	0.0428	0.0178
77	0.1241	0.0266	0.0559	0.0426	0.0158

Decay characteristics were based on multicompartmental models.[11–15] Normal *WM* had a T_2 spectrum with three main peaks at 10, 80, and 100 ms, with the short T_2 component representing water in myelin, the middle T_2 component representing water in axons, and the long T_2 component representing intracellular and extracellular water. Lesions contained only two exponential components. Myelin was assumed to be damaged.[16,17] Gaussian random noise was added to decay signals. The SNR of the noisy simulation data was about 80 dB at the first echo time. The longer echo time, the lower SNR because of signal intensity attenuation.

II.C. Denoising in the temporal-domain: Model-based approach

A model for decay signals was used to reduce noise in the temporal-domain. Since the decay rate of the MR temporal signal at each location is governed by MR physics known as $T_2(*)$ relaxation, the decay signal can be modeled with an exponential function.[12,13,16] If a single voxel contains different tissues, then the decay signal can be modeled with a multi-exponential function.[14,15] Therefore, the decay signal was fit into a specific multi-exponential function by a minimization process, such as a least squares algorithm. Noise was reduced during this fitting process, and this reduction translated into reduction of noise in the spatial domain. The primary curve fit algorithm used in this paper was a nonnegative least squares algorithm (NNLS).[18,19] The NNLS algorithm assumes that the decay signal consists of several exponential decay components and estimates each decay component by minimizing the error between modeled multi-exponential signal and the measured decay signal, using Eq. (2) with a nonnegativity constraint.

$$\min_s \|A \cdot s - y\|_2^2, \quad \text{where} \quad s \geq 0, \tag{2}$$

where y is the acquired decay signal and s is the $T_2(*)$ spectrum. A is the system matrix which transforms the $T_2(*)$ spectrum, s, into the acquired decay signal, y ($A_{ij} = e^{-TE_i}/T_{2j}(*)$ and $y = A \cdot s$).

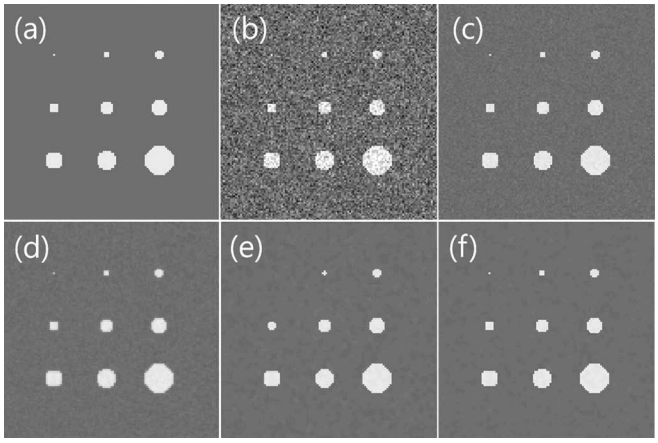

FIG. 3. Comparison of spatiotemporally denoised images at $TE = 22$ ms. True image (a), noisy image (b), and temporally denoised images with model-based method (c), and spatially filtered results of (c) with LPF (d), MF (e), and ADF (f).

II.D. Comparison of the model-based approach and the filtering approach in the temporal-domain

The proposed denoising method was compared to conventional filters in the temporal-domain. Multi-echo images in experiments and simulations were filtered in the temporal-domain using the three conventional filters: LPF, MF, and ADF. In the simulation, the standard deviation of the

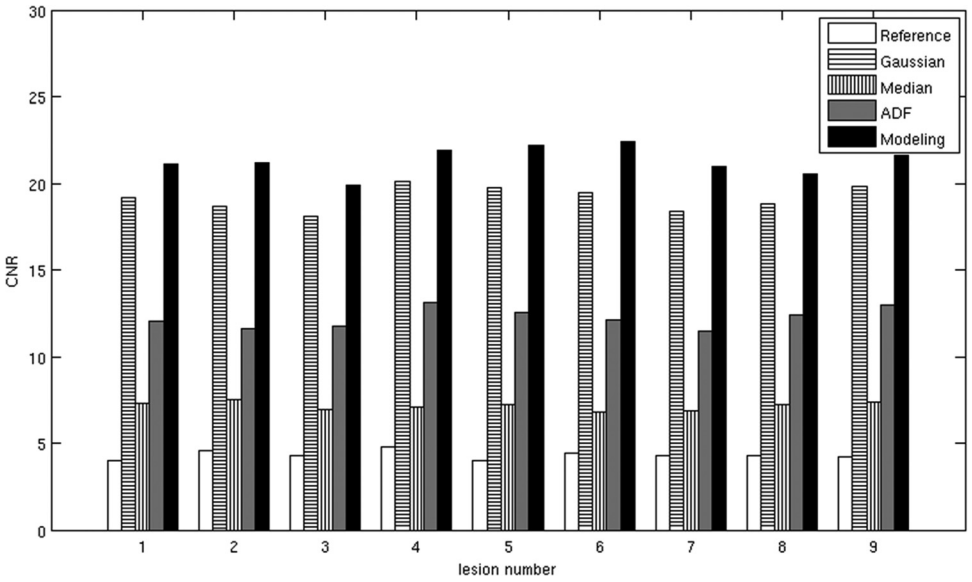

FIG. 2. CNR of the temporally denoised images at nine lesions. The model-based method showed the highest CNRs for all lesions.

TABLE II. MSE of the spatiotemporally denoised images at three different echo times.

TE (ms)	Reference	Modeling	Modeling + LPF	Modeling + MF	Modeling + ADF
27	0.1235	0.0228	0.0190	0.0176	0.0073
52	0.1242	0.0178	0.0136	0.0120	0.0056
77	0.1241	0.0158	0.0108	0.0082	0.0052

Gaussian function for LPF was 6.06 and the kernel length was 35. For MF, the kernel length was 11. For ADF, the parameter κ was set to five times the standard deviation of the noise, and 30 iterations were used for sufficient denoising effect. All parameters were selected to produce the best filtering results. Temporally filtered images were compared to the denoised images using the model-based method.

Visual comparisons were made on images at specific echo time = 22 ms. For quantitative comparisons, MSE and CNR were calculated and compared for focal lesions in the simulations. CNR was defined as follows:

$$\mathrm{CNR} = |S_{\mathrm{lesion}} - S_{WM}|/\sigma_{WM}, \tag{3}$$

where S_{lesion} and S_{WM} are the mean signal intensities in lesions and surrounding normal *WM*, respectively. σ_{WM} is the standard deviation of the signal intensities in the surrounding normal *WM*.

III. RESULTS

Figure 1 shows the true image (a), and the noisy image (b) from the synthetic dataset with $SNR = 80$ dB at $TE = 22$ ms, and denoised images by temporal filtering with LPF (c), MF (d), ADF (e), and the model-based method (f) on the temporal-domain. In addition, images denoised by each filter in the spatial domain but not the temporal-domain are shown in a box (c–e) to show spatial artifacts caused by conventional "spatial" filters; an image at a specific echo time of 22 ms was spatially filtered. Spatial LPF reduced noise, but caused a blurring effect and smoothed lesion edges. The single-pixel lesion was not identifiable. MF also performed poorly. The boundaries of the lesions were smoothed, and the single-pixel lesion was not identifiable. Furthermore, the background appeared to contain several patches of objects where it should have been homogeneous. ADF appeared to be better, but failed to preserve accurate lesion boundaries. All spatial artifacts were caused by a high noise level in a single MR image at a single echo time and by nonlinear properties of the spatial filters. In contrast to the spatial filtering approach, denoising methods performed in the temporal-domain effectively reduced noise without causing noticeable artifacts. This result was a natural consequence of the independent, pixel-by-pixel denoising process, and the use of multiple image sets in the denoising procedure. By visual comparison of the denoised results in the temporal-domain, the denoised image by the model-based approach gave the best performance of all methods.

For quantitative comparison, MSEs were calculated for the original noisy image and the denoised images by conventional filter and the model-based method in the temporal-domain (Table I). In all cases, the model-based method resulted in the lowest MSEs. CNRs were measured for nine lesions and are compared in Fig. 2. The model-based method also resulted in the highest CNRs. The second highest CNRs were obtained when Gaussian LPF was applied to temporal decay signals. MF and ADF resulted in lower CNRs than LPF. We also investigated the synergistic effect of combining both temporal and spatial filtering. After performing the model-based denoising on the temporal-domain, conventional spatial filters were applied to the temporally denoised image for additional noise reduction.

Figure 3 compares the images at $TE = 22$ ms that were denoised in the spatiotemporal-domain: (a) the true image, (b) the noisy image, and (c) the temporally denoised image

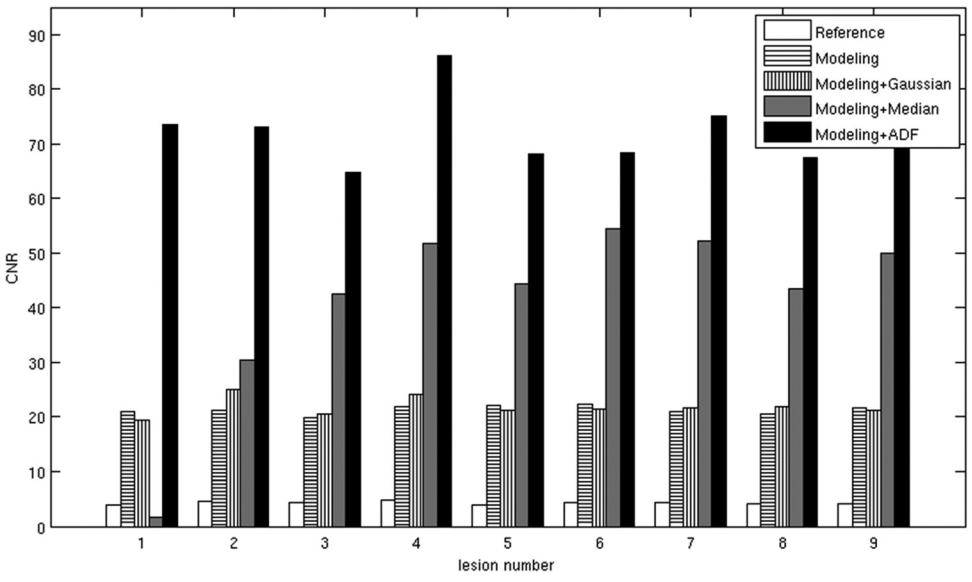

FIG. 4. CNR of spatiotemporally denoised images at nine lesions. The spatially denoised image with ADF showed the highest CNRs for all lesions.

with the model-based method, and the spatially filtered results of (c) with (d) LPF, (e) MF, and (f) ADF. Spatial LPF sufficiently removed the residual noise, but smoothed out lesion boundaries. MF preserved lesion sharp edges better than LPF, but its nonlinear process distorted some boundaries, and the single-pixel lesion was smoothed and not identifiable. ADF effectively suppressed noise without noticeable distortion, giving an almost true image. MSEs were calculated for the denoised images in the spatiotemporal-domain (Table II). In all cases, ADF resulted in the lowest MSEs. Figure 4 compares CNRs for all lesions for each filtered image. ADF showed the highest CNRs for all lesions. MF showed the second highest CNRs except for the small lesion 1, for which the CNR was lower than other methods because the nonlinear process of MF smoothed out the single-pixel lesion.

Figure 5 shows the *in vivo* image acquired at 38.7 ms by conventional GRE sequence (a), at 38.73 ms by MGRE sequence (b); and a temporally denoised image of (b) by the model-based method (c). The spatial noise in the MGRE was substantially reduced with no spatial artifacts. The contrast between white and gray matter was better in the model-based method and the noise level was lower than the GRE sequence. This indicated the effectiveness of our proposed approach. In addition to improved SNR, the proposed approach resulted in multiple high-quality $T_2(*)$ contrast images [Figs. 5(d)–5(f)]. In contrast, the conventional acquisition method normally produces a single $T_2(*)$ contrast image [Fig. 5(a)]. Figures 5(d)–5(f) shows denoised images at $TE = 11.18$, 33.22, and 60.77 ms. Each shows that contrast between tissues with high SNR had a comparable or better SNR than with conventional GRE.

Figures 6(a)–6(c) shows magnified view of images in Figs. 5(a)–5(c). The denoising effect is clearly seen for the proposed method. Figures 6(d)–6(f) are the denoised images with additional spatial filtering applied with LPF, MF, and ADF. Further noise reduction was observed, but at the cost of introducing spatial artifacts.

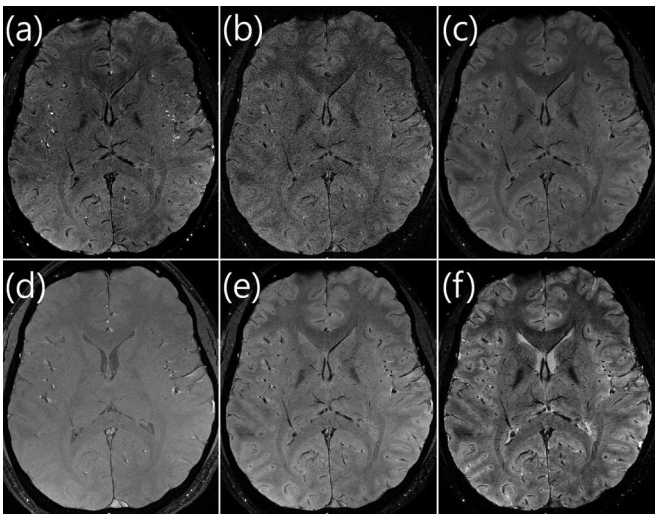

FIG. 5. Comparison of acquired *in vivo* images. Conventional GRE sequence at $TE = 38.7$ ms (a), MGRE sequence at $TE = 38.73$ ms (b), denoised image of (b) with model-based method (c), and other denoised images of MGRE data at $TE = 11.18$ ms (d), $TE = 33.22$ ms (e), and $TE = 60.77$ ms (f).

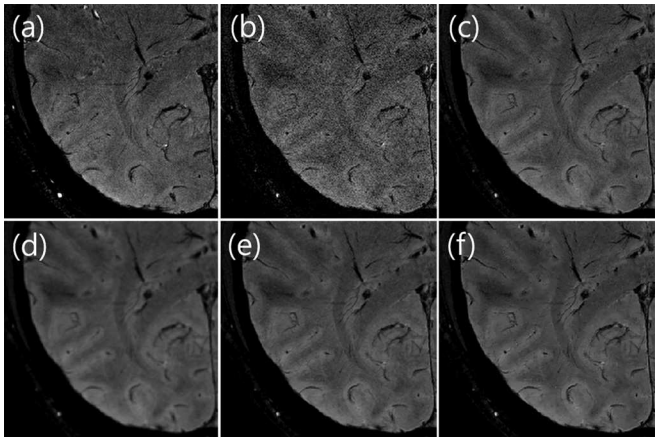

FIG. 6. Comparison of spatiotemporally denoised *in vivo* images at $TE = 38.73$ ms. Acquired image with GRE sequence at 38.7 ms (a), MGRE sequence at 38.73 ms (b), denoised image with the model-based method (c), and spatially filtered results of (c) with LPF (d), MF (e), and ADF (f).

IV. CONCLUSIONS

This study demonstrated that denoising in the temporal-domain of multi-echo MR images using conventional filters or a model-based method substantially reduced spatial noise without introducing blurring or artificial appearances. Our proposed method produced multiple high-SNR $T_2(*)$ contrast images. Simulations and *in vivo* experiments showed the effectiveness of our proposed temporal denoising approach. The model-based method was more effective at reducing noise than conventional filters applied to the temporal-domain. Spatial artifacts such as blurring or staircasing effects were not observed in temporally denoised images. This was a natural consequence since the denoising methods did not use spatial information. Simulation studies showed that the model-based method had lower MSE and highest CNR than conventional filters.

The main reason for SNR improvement by the proposed temporal denoising method was the large number of images used in the denoising process. For example, temporal LPF can be regarded as a weighted averaging of multiple images that result in SNR improvement. An extreme case of LPF would be a simple averaging of all images. This extreme case would result in a single contrast image with high SNR improvement, but one that would have lost valuable temporal information. This is a concern for the proposed temporal denoising scheme. Temporal information might be lost because of temporal denoising, similar to the smoothing of details or edges with a spatial filter. This concern has been discussed before. For example, Haider *et al.* introduced a "temporal footprint" parameter to characterize time-resolved view-shared sequences for dynamic contrast-enhanced MR angiography.[20] A long temporal footprint represents a long duration over which views used for a single image are acquired,[20] leading to low temporal fidelity. In our case, the temporal footprint might increase because of temporal denoising, since several images

at different echo times were used to produce a final denoised image. However, the original decay signals in multi-echo images change very slowly, following exponential decay pattern; therefore, no sharp edges or boundaries are lost by LPF or the model-based method. Consequently, the amount of temporal information lost from the increase of the temporal footprint in multi-echo MR images would be very small.

The model-based method uses a multi-exponential model for decay signals since the MR signal at a specific voxel follows a multi-exponential decay, or $T_2(*)$ relaxation. Noisy decay signals were fitted to this model using the NNLS algorithm. Spatial noise was substantially reduced in this fitting process. This method resulted in lower MSEs and higher CNRs than other denoising methods using conventional filters in the temporal-domain, without introducing spatial artifacts. The visibility of small focal lesions and fine structures was substantially improved.

One interesting result in the simulation studies was that temporal LPF performed better than the other nonlinear filters applied to the temporal-domain. In general, when applied to the spatial domain of images, MF and ADF performed better than LPF for noise reduction and ability to preserve sharp edges. However, they tended to introduce artificial appearances such as a staircasing artifacts or flat zones in smooth areas because of their nonlinear process. In other words, they tended to produce artifactual discontinuity when applied to continuous signals. Therefore, when they were applied to the smooth decay signals of multi-echo MR images, they also produced artifactual discontinuity over the smoothly varying multi-exponential decay signals, which introduced error. This nonlinear filter error resulted in larger MSEs and lower CNRs than seen with LPF, which did not introduce discontinuity making it superior to the multi-exponential decay signals.

The multi-exponential model was valid for most cases in the multi-echo MR images. However, in certain conditions, a nonexponential decay might occur in the gradient-echo based images from field inhomogeneity. For example, a local field gradient (LFG) along the slice direction could induce nonexponential signal decay in regions with moderate or severe field inhomogeneity. Therefore, a multi-exponential model might not be valid in these regions.[21,22] In such cases, a sinc or quadratic function that approximates the LFG-induced decay can be incorporated into the original exponential model.[23]

In conclusion, this study demonstrated that denoising approaches in the temporal-domain can effectively reduce noise in the spatial domain without introducing spatial artifacts. Therefore, the method proposed here can increase the spatial SNR in each image with different $T_2(*)$ weights in multi-echo MR images, leading to multiple high-quality $T_2(*)$ contrast images.

ACKNOWLEDGMENTS

The authors thank Siemens for pulse sequence support and Yoonho Nam for assistance with data acquisition. This research was supported by Basic Science Research Program through the National Research Foundation of Korea (NRF) funded by the Ministry of Education, Science and Technology (2011-0025574).

[a]Author to whom correspondence should be addressed. Electronic mail: dosik.hwang@yonsei.ac.kr. Telephone: + 82) 2-2123-5771; Fax: + 82) 2-313-2879.

[1]A. M. Wink and J. B. Roderick, "Denoising functional MR images: A comparison of wavelet denoising and Gaussian smoothing," IEEE Trans. Med. Imaging **23**, 374–387 (2004).
[2]K. Ying, B. D. Clymer, and P. Schmalbrock, "Adaptive filtering for high resolution magnetic resonance images," J. Magn. Reson. Imaging **6**, 367–377 (1996).
[3]A. A. Samsonov and C. R. Johnson, "Noise-adaptive nonlinear diffusion filtering of MR images with spatially varying noise levels," Magn. Reson. Med. **52**, 798–806 (2004).
[4]Y. P. Du, R. Chu, D. S. Hwang, M. S. Brown, B. K. Kleinschmidt-DeMasters, D. Singel, and J. H. Simon, "Fast multi-slice mapping of the myelin water fraction using multi-compartment analysis of T_2* relaxation at 3 tesla—A preliminary post-mortem study," Magn. Reson. Med. **58**, 865–870 (2007).
[5]D. S. Hwang, D. H. Kim, Y. P. Du, "*in vivo* multi-slice mapping of myelin water content using T_2* decay," Neuroimage **52**, 198–204 (2010).
[6]V. Brainovicha, U. Sabatinib, and G. E. Hagberga, "Advantages of using multiple-echo image combination and asymmetric triangular phase masking in magnetic resonance venography at 3 T," Magn. Reson. Imaging **27**, 23–37 (2009).
[7]Y. P. Du, Z. Jin, Y. Hu, and J. Tanabe, "Multi-echo acquisition of MR angiography and venography of the brain at 3 tesla," J. Magn. Reson. Imaging **30**, 449–454 (2009).
[8]U. Dorenbeck, A. G. Schreyer, J. Schlaier, P. Held, S. Feuerbach, and J. Seitz, "Degenerative disease of the cervical spine: Comparison of a multi-echo data image combination sequence with a magnetization transfer saturation pulse and cervical myelography and CT," Neuroradiology **46**, 306–309 (2004).
[9]M. R. Schmid, C. W. A. Pfirrmann, P. Koch, M. Zanetti, B. Kuehn, and J. Hodler, "Imaging of patellar cartilage with a 2D multiple-echo data image combination sequence," AJR, Am. J. Roentgenol. **184**, 1744–1748 (2005).
[10]M.A. Griswold, P. M. Jakob, R. M. Heidemann, M. Nittka, V. Jellus, J. Wang, B. Kiefer, and A. Haase, "Generalized autocalibrating partially parallel acquisition (GRAPPA)," Magn. Reson. Med. **47**, 1202–1210 (2002).
[11]M. D. Does and J. C. Gore, "Compartmental study of T_1 and T_2 in rat brain and trigeminal nerve *in vivo* ," Magn. Reson. Med. **47**, 274–283 (2002).
[12]J. L. Lancaster, T. Andrews, L. J. Hardies, S. Dodd, P. T. Fox, "-Three-pool model of white matter," J. Magn. Reson. Imaging. **17**, 1–10 (2003).
[13]T. Andrews, J. L. Lancaster, S. Dodd, C. Contreras-Sesvold, and P. T. Fox, "Testing the three-pool white matter model adapted for use with T_2 relaxometry," Magn. Reson. Med. **54**, 449–454 (2005).
[14]K. Wachowicz and R. E. Snyder, "Assignment of the T_2 components of amphibian peripheral nerve to their microanatomical compartments," Magn. Reson. Med. **47**, 239–245 (2002).
[15]H. L. Valentine, M. D. Does, V. Marshall, E. G. Tonkin, and W. M. Valentine, "Multicomponent T_2 analysis of dithiocarbamate-mediated peripheral nerve demyelination," Neurotoxicology **28**, 645–654 (2007).
[16]D. S. Hwang and Y. P. Du, "Improved myelin water quantification using spatially regularized non-negative least squares algorithm," J. Magn. Reson. Imaging **30**, 203–208 (2009).
[17]C. Laule, E. Leung, D. K. Li, A. L. Traboulsee, D. W. Paty, A. L. MacKay, and G. R. Moore, "Myelin water imaging in multiple sclerosis: Quantitative correlations with histopathology," Mult. Scler. **12**, 747–753 (2006).
[18]C. L. Lawson and R. J. Hanson, *Solving Least Squares Problems* (Prentice-Hall, Englewood Cliffs, New Jersey, 1974).
[19]S. W. Provencher, "A constrained regularization method for inverting data represented by linear algebraic or integral equations," Comput. Phys. **27**, 213–227 (1982).

[20]C. R. Haider, H. H. Hu, N. G. Campeau, J. Huston III, and S. J. Riederer, "3D high temporal and spatial resolution contrast enhanced MR angiography of the whole brain," Magn. Reson. Med. **60**, 749–760 (2008).
[21]D. A. Yablonskiy, "Quantitation of intrinsic magnetic susceptibility related effects in a tissue matrix: Phantom study," Magn. Reson. Med. **39**, 417–428 (1998).
[22]R. Wirestam, O. Thilmann, L. Knutsson, I. M. Bjorkman-Burtscher, E. M. Larsson, and F. Stahlberg, "Comparison of quantitative dynamic susceptibility-contrast MRI perfusion estimates obtained using different contrast-agent administration schemes at 3T," Eur. J. Radiol. **75**, e86–e91 (2010).
[23]M. A. Fernandez-Seara and F. W. Wehrli, "Postprocessing technique to correct for background gradients in image-based R_2* measurements," Magn. Reson. Med. **44**, 358–366 (2000).